Physica E 44 (2011) 530–533

Contents lists available at SciVerse ScienceDirect

Physica E

journal homepage: www.elsevier.com/locate/physe

Quantum hall effect in inhomogeneous trilayer graphene

Cayetano Cobaleda [a], Francesco Rossella [b,*], Sergio Pezzini [a,b], Enrique Diez [a], Vittorio Bellani [b], Duncan Maude [c], Peter Blake [d]

[a] Laboratorio de Bajas Temperaturas, Universidad de Salamanca, E-37008 Salamanca, Spain
[b] Dipartimento di Fisica "A. Volta", Università degli Studi di Pavia, I-27100 Pavia, Italy
[c] Laboratoire National des Champs Magnétiques Intenses, CNRS-UJF-INSA-UPS, F-38042 Grenoble, France
[d] Graphene Industries Ltd., Manchester Centre for Mesoscience & Nanotechnology, Oxford Road, Manchester M13 9PL, United Kingdom

ARTICLE INFO

Article history:
Received 25 July 2011
Received in revised form
22 September 2011
Accepted 7 October 2011
Available online 13 October 2011

ABSTRACT

We have performed magneto-transport experiments in trilayer graphene, at temperatures between 2 and 190 K and magnetic fields up to 22 T. Here we report the integer quantum Hall effect in trilayer graphene, showing the quantum Hall plateau at $\nu=6$ and studying its temperature dependence. The symmetry properties of the resistance in the quantum Hall regime and at low magnetic fields are also investigated. The measurements obey the reciprocity relation, and reveal new symmetries that relate the resistances measured with different contact configurations.

1. Introduction

Graphene is the subject of numerous investigations due to its unique electronic and lattice properties, which are interesting both conceptually and for several applications [1–5]. The unique electronic band structure of graphene leads to fascinating phenomena, exemplified by the massless Dirac fermion physics and the anomalous quantum Hall effect (QHE) [1–8]. In graphene a pseudospin quantum number plays the role of spin, and the pseudospin splitting is exactly equal to the orbital splitting; Accordingly, we can see the nth LL as composed of the degenerate pseudospin-up and pseudospin-down states of the LL n and $n-1$, respectively, and the resulting series of the quantum Hall plateaus is $\nu=\pm 2,\ \pm 6,\ \pm 10,\ \pm 14,\ \ldots$ for monolayer graphene and $\nu=\pm 4,\ \pm 8,\ \pm 12,\ \pm 16,\ \ldots$ for bilayer graphene [9]. The experimental observation of these unconventional series for the QHE in monolayer [6,7] and bilayer [8] graphene provided the milestone that paved the way for the subsequent investigations of the electronic properties of graphene and graphene multilayers. Furthermore, the presence of the QHE in trilayer graphene (TLG) is a subject of great fundamental interest since the band structure of TLG strongly depends on the interlayer stacking sequence [10–18].

In this paper we show the presence of the $\nu=6$ integer quantum Hall plateau in trilayer graphene. The symmetries of the resistance measured with the four-terminal configuration in the quantum Hall regime reveal a rather intriguing behavior. Upon the reversal of the magnetic field, we observe the non-parity of the longitudinal resistivities, which partially reproduces the behavior previously observed in a mesoscopic 2D electron gas [19] and more recently in graphene [20,21]. Our results are explained taking into account the inhomogeneities observed in the sample.

2. Material and methods

The TLG flake investigated here has been fabricated by means of mechanical exfoliation of natural graphite before being placed onto a Si wafer with a 300 nm SiO_2 top layer. The TLG was identified using optical microscopy and micro-Raman spectroscopy. Fig. 1 (top panel) shows an optical image of the selected TLG flake, together with the outline of the Hall bar to be fabricated. The selected flake was processed to form a Hall bar geometry using photo-lithography (LaserWriter, 405 nm wavelength) with a "lift-off" process, and a bilayer stack of PMGI and S1805 was used for the resist. The contacts (50 Å nm of Ti followed by 500 Å of Au) were deposited via electron-beam evaporation while the undesired parts of the flake were removed using oxygen/argon plasma etching. The remaining TLG was protected with PMMA. The aspect ratio (W/L) of the fabricated Hall bar was 0.62.

We measured the Raman scattering spectrum of the TLG Hall bar at room temperature, using a micro-Raman set-up with laser light excitation at 1.96 eV with $\sim$1 mW/μm^2 power density. We used 50× and 100× objectives, with a corresponding laser spot area of approximately 4 μm^2 and 1 μm^2, respectively; the spatial resolution of the setup in the xy plane was approximately 0.5 μm.

* Corresponding author.
E-mail address: francesco.rossella@unipv.it (F. Rossella).

1386-9477/$ - see front matter © 2011 Elsevier B.V. All rights reserved.
doi:10.1016/j.physe.2011.10.007

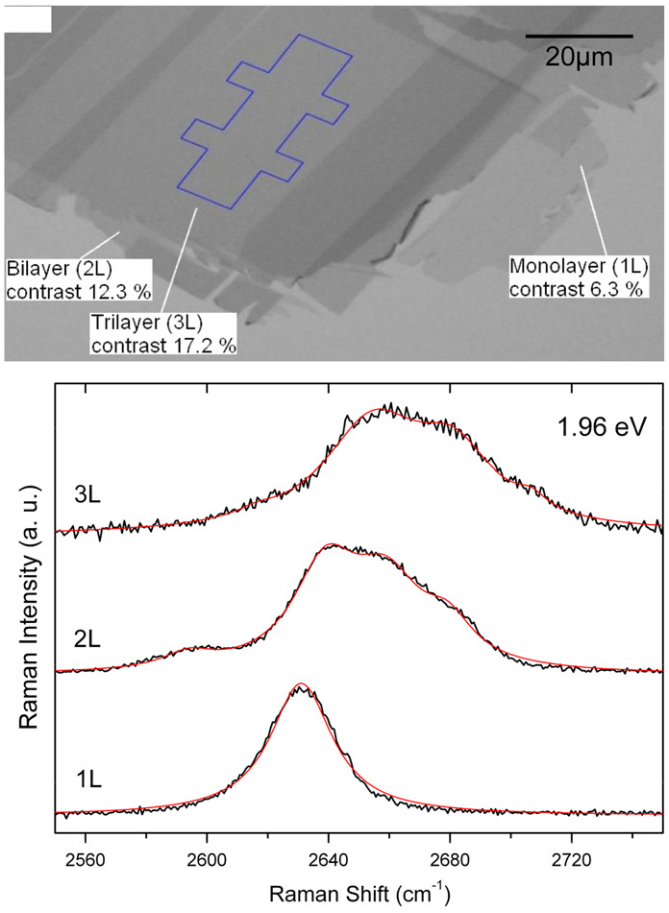

Fig. 1. Top panel: optical image of the TLG flake; the region where the Hall bar is to be processed is outlined. Bottom panel: Raman spectrum of the TLG device used in this work (3L), together with for comparison, the Raman spectra of monolayer (1L) and bilayer (2L); Red curves represent the (multi)-Lorentzian fitting. (For interpretation of the references to colour in this figure legend, the reader is referred to the web version of this article.)

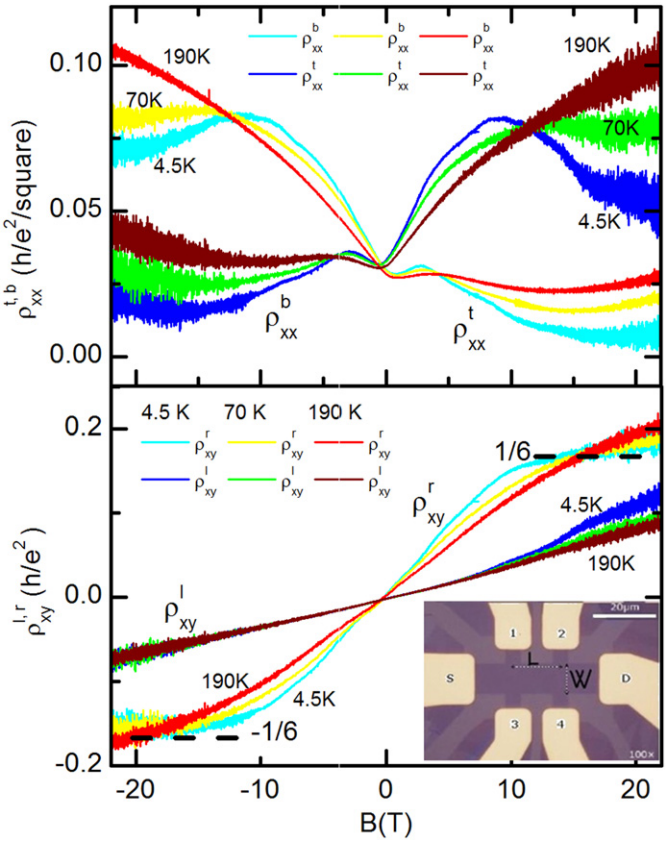

Fig. 2. Hall (ρ_{xy}) and longitudinal resistivities (ρ^t_{xx} and ρ^b_{xx}), in fundamental units, versus B at temperatures of 4.5, 70 and 190 K. The quantum Hall plateau at $\nu=\pm 6$ corresponding to $\rho^r_{xy}=h/6e^2$ is visible up to 70 K. We note that the longitudinal resistivities measured on "top" and "bottom" edges of the Hall bar show a remarkable symmetry relation at high magnetic fields, $\rho^t_{xx}(-B)\cong\rho^b_{xx}(B)$. The inset shows an optical image of the TLG device used for magneto-transport experiments. The electrodes for current injection (S and D), the geometrical factors (L and W) and the measuring electrodes (1–4) are labeled.

Fig. 1 (bottom panel) shows the characteristic Raman scattering "2D" band of the sample under study, and of monolayer (1L) and bilayer (2L) graphene for comparison. Lui et al. [22] recently showed that the peculiar shape of the 2D Raman band provides a powerful tool for the analysis of the stacking in TLG. The Raman spectrum of our graphene device reported in Fig. 1 exhibits the multi-component feature characteristic of TLG, and according to Ref. [22] suggests the presence of a Bernal-stacking ABA.

The sample was placed into a ^{4}He cryostat with a variable temperature insert with an operating range of 2–300 K. Four probe measurements were carried out using standard ac lock-in techniques. A voltage of 5 V with frequencies below 15 Hz was applied to a 100 MΩ in-series resistance, providing an excitation current $I=50$ nA from contact S to D (see inset in Fig. 2). We employed different pre-amplifiers with a gain of ~100 measuring simultaneously the voltage drop V_{1-3}, V_{1-2} and V_{3-4} between the contact pairs 1–3, 1–2 and 3–4 as labeled in the inset of Fig. 2. A 10 MW magnet was used to apply magnetic fields up to 22 T perpendicularly to the TLG.

3. Results and discussion

To facilitate the discussion, we define the "left" Hall resistivity as $\rho^l_{xy}=V_{1-3}/I$, the "right" Hall resistivity as $\rho^r_{xy}=V_{2-4}/I$, and the longitudinal resistivity for the "top" contacts as $\rho^t_{xx}=V_{1-2}/L)/(I/W)$ and for the "bottom" contacts as $\rho^b_{xx}=(V_{3-4}/L)/(I/W)$. In Fig. 2 we show the longitudinal ($\rho^{t,b}_{xx}$) and Hall resistivities ($\rho^{l,r}_{xy}$) as functions of the magnetic field.

From the longitudinal and Hall resistances at low magnetic field, we can extract the 2D carrier density n and mobility μ of the sample at different temperatures. The carrier density increases with increasing temperature, as expected for the semi-metallic TLG [10]. As can be observed in Fig. 2 the two Hall resistivities are different from each other in several aspects. First of all, the "left" Hall resistivity has a linear dependence on the magnetic field whereas the "right" Hall resistivity shows the QHE with the presence of the $\nu=6$ plateau. From the slope of the "left" Hall resistivity we obtain, at 4.5 K, the value $n^l=6.43\times10^{12}$ cm^{-2} for the carrier density on the *left* side of the Hall bar. Following the same procedure for the "right" Hall resistivity we obtain the value of the carrier density on the *right* side of the Hall bar $n^r=2.04\times10^{12}$ cm^{-2}. Thus, we can conclude that there is an evident inhomogeneity present in our sample, since the carrier densities at different sides of the Hall bar differ by a factor of 3 ($n^l\sim3n^r$).

On the *right* side of the Hall bar, the mobility of our sample changes from $\mu=3750$ cm^2/Vs at 4.5 K to $\mu=3173$ cm^2/Vs at 190 K. The mobility of our TLG sample is sufficient to reach the QHE regime at magnetic fields above 3 T, as evidenced by the observation of well developed plateaus at $\rho_{xy}=\pm h/6e^2\sim\pm0.16h/e^2$ corresponding to $\nu=6$ or $\nu=-6$ depending upon the polarity of the magnetic field. We can see that the bottom longitudinal resistivities measured at different temperatures cross at B~12.7 T. This value is

in good agreement with the expected crossing point for a 2D system with our carrier density ($\nu = nh/eB$). Indeed, for the density $n = 2.04 \times 10^{12}\ \mathrm{cm}^{-2}$ of our sample at 4.5 K we calculate a filling factor $\nu = 6$ at a magnetic field of $B = nh/e\nu \sim 14$ T. We can perform the same analysis for the *left* side of the Hall bar, and, since the carrier density is higher than the density at the *right* side of the Hall bar, the magnetic field at which the $\nu = 6$ plateau should appear is 3 times bigger, i.e. $B \sim 42$ T. This is the reason why the plateau is not reached for the "left" Hall resistivity.

There is yet another peculiarity that needs to be explained. In Fig. 2 it can be seen that the longitudinal resistivities are not symmetric with the magnetic field but they map onto each other under the reversal of the magnetic field, i.e. $\rho_{xx}^{t,b}(B) \neq \rho_{xx}^{t,b}(-B)$ and $\rho_{xx}^{t,b}(B) \cong \rho_{xx}^{b,t}(-B)$.

This behavior is extremely robust since it survives for temperatures as high as 190 K. Indeed, as the temperature increases, the resistivity curve changes while the inversion symmetry persists. The magneto-transport properties exhibited by the top and bottom edges of our TLG device expressed by the relation $\rho_{xx}^{t,b}(B) \cong \rho_{xx}^{b,t}(-B)$ holds even at very low magnetic fields. This inversion symmetry has been previously observed also in mesoscopic Hall bars in semiconductor 2D electron gases [19] and can be attributed to an inhomogeneity in the sample, which leads to a non-zero gradient in the carriers density along the Hall bar, as proposed by Karmakar et al. [23]. In accordance with their model, the perpendicular magnetic field would induce a non uniform accumulation of charge carriers at the boundaries of the sample, which causes the current density to be spatially inhomogeneous. In this picture we name ρ_{xx} and ρ_{xy} the longitudinal and Hall resistivities unaffected by the sample's inhomogeneity, which are respectively even and odd in B, we can write the resistivities measured with our contact geometry as

$$\rho_{xx}^{t,b} = \left(\rho_{xx} \pm \rho_{xy}\beta\frac{W}{2}\right) = \frac{L}{W}R_{xx}^{t,b} \tag{1a}$$

$$\rho_{xy}^{l,r} = \rho_{xy}\left(1 \pm \beta\frac{L}{2}\right) = R_{xy}^{l,r} \tag{1b}$$

where β is a phenomenological parameter that can depend on the magnetic field and on the temperature [23] and which is even in the magnetic field. Relations Eqs. 1a and 1b imply that the relation

$$\Delta R_{xx} = R_{xx}^{t} - R_{xx}^{b} = R_{xy}^{r} - R_{xy}^{l} = \Delta R_{xy} = \Delta R$$

will hold independently of the magnetic field. In the case of an homogeneous sample $\Delta R = 0$ but ΔR will have a non-zero value if the sample is not homogeneous, as it is shown in Fig. 3.

Since at low magnetic field the Hall resistivity can be approximated by $\rho_{xx} = B/en$, the parameter βL is given by (from Eq. 1b) $\beta L = (n^{l} - n^{r}/(n^{l} + n^{r})/2)$.

Thus, βL is a percentage quantity that expresses the level of inhomogeneity present in the sample. Since $n^{l} \sim 3n^{r}$, we have that $\beta L \approx 1$, so we conclude that the difference of the carrier densities at both sides of the Hall bar is of the same order than the mean carrier density.

As shown in Fig. 3, this relation is fully consistent with our data. This lends strong support to the hypothesis that the observed behavior of our sample can be attributed to non homogenous carrier density and we will therefore continue our analysis using the model of Karmakar et al. Accordingly, the true longitudinal resistivity can be calculated performing an average between the "top" and "bottom" longitudinal resistivities, which effectively takes into account only their symmetric parts, i.e.

$$\rho_{xx}(B) = [\rho_{xx}^{t}(B) + \rho_{xx}^{b}(B)]/2 = [\rho_{xx}^{t,b}(B) + \rho_{xx}^{b,t}(-B)]/2$$

As far as the Hall resistivities are concerned, we cannot proceed in a similar way to analyze the QHE since the density on the *left* side of the Hall bar is three times larger than the density on the *right* side of the Hall bar so that we must treat them separately. We focus on ρ_{xy}^{r}, since for the available magnetic field range, the filling factor $\nu = \pm 6$ can only be achieved at the *right* side of the Hall bar. For simplicity, in the following we will refer to ρ_{xy}^{r} as ρ_{xy}.

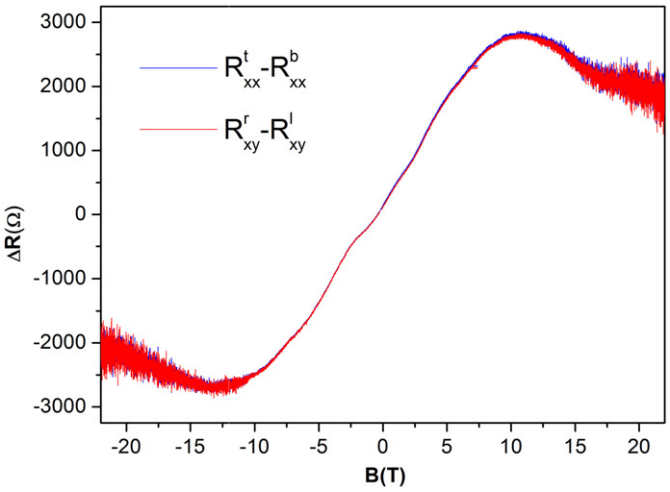

Fig. 3. Difference of the two longitudinal resistances (blue: "top" minus "bottom") and the two Hall resistances (red: "right" minus "left") at $T = 4.5$ K. (For interpretation of the references to colour in this figure legend, the reader is referred to the web version of this article.)

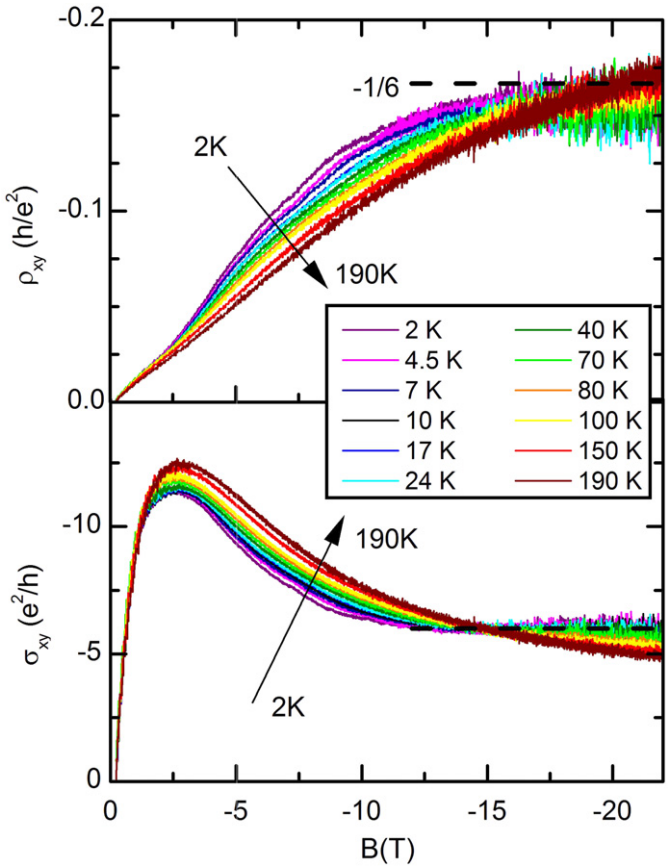

Fig. 4. Hall resistivities (top panel) and Hall conductivities (bottom panel) reported in fundamental units B at temperatures between 2 and 190 K. The quantum Hall plateau at $\nu = -6$ with $\sigma_{xy} = -6e^2/h$ is clearly evident at temperatures < 70 K.

Once this analysis is performed, we calculate the components of the conductivity tensor by means of the usual relations

$$\sigma_{xx} = \frac{\rho_{xx}}{\rho_{xx}^2 + \rho_{xy}^2} \tag{2a}$$

$$\sigma_{xy} = \frac{\rho_{xy}}{\rho_{xx}^2 + \rho_{xy}^2} \tag{2b}$$

In Fig. 4 the components of the conductivity tensor σ_{xy} (calculated by means of Eq. 2b) at temperatures from 2 K up to 190 K as a function of the magnetic field are displayed in the bottom panel. In the top panel the resistivities are also plotted for comparison. Concerning σ_{xy}, we can see a plateau at $\sigma_{xy}=6e^2/h$ corresponding to $\rho_{xy}=-h/6e^2\sim-0.16\mathrm{h/e}^2$. Some features observed at lower magnetic field suggest the presence of other unresolved quantum Hall plateaus. The Shubnikov-de Haas oscillations for our sample mobility are expected to begin for $B\sim3$ T, so we can take this point as the beginning of the QHE regime. As mentioned above, the existence of a series of quantum Hall plateaus in TLG at filling factors $\nu=\pm6,\ \pm10,\ \pm14,\ \ldots$ has been theoretically predicted [11]. Therefore, when the density is that which corresponds to the density at 4.5 K, we should expect the $\nu=10$ QH plateau at $B\sim7.7$ T and the $\nu=14$ at $B\sim5.5$ T. In Fig. 4 the Hall conductivity takes values close to $-10e^2/h$ for magnetic fields between 5 T and 8 T. Furthermore, at the lowest temperatures, the Hall resistivities present a change in their Hall slopes at $B\sim7$ T with $\rho_{xy}\sim-0.10h/e^2$ almost constant for 0.3 T, compatible with an unresolved plateau at $\nu=10$. Experiments at lower temperatures and with higher mobility samples should allow to evidence exhibit additional more clearly resolved QH plateaus.

4. Conclusions

In conclusion, we have measured the quantum Hall effect in a trilayer graphene Hall bar observing the presence of the $\nu=6$ plateaus. We study its temperature dependence, which is compatible with the expected features in the quantum Hall regime. We also observed symmetry properties upon the reversal of the magnetic field, which reveal a remarkable agreement with the model based on a carrier density gradient along the device.

Acknowledgment

This work was supported by the projects Cariplo Foundation QUANTDEV, MEC FIS2009-07880, PPT310000-2009-3, JCYL SA0-49A10-2, the FPU program by MEC and by EuroMagNET II under the EU Contract no. 228043. The authors thank J.M. Cervero, G.P. Parravicini, L. Brey and F. Guinea for the useful discussion.

References

[1] A.K. Geim, K.S. Novoselov, Nat. Mater. 6 (2007) 183.
[2] A.H. Castro Neto, F. Guinea, N.M.R. Peres, K.S. Novoselov, A.K. Geim, Rev. Mod. Phys. 81 (2009) 109.
[3] M.A.H. Vozmediano, M.I. Katsnelson, F. Guinea, Phys. Rep. 496 (2010) 109.
[4] A. Cresti, N. Nemec, B. Biel, G. Niebler, F. Triozon, G. Cuniberti, S. Roche, Nano Res. 1 (2008) 361.
[5] N.M.R. Peres, Rev. Mod. Phys. 82 (2010) 2673.
[6] K.S. Novoselov, A.K. Geim, S.V. Morozov, D. Jiang, M.I. Katsnelson, I.V. Grigorieva, S.V. Dubonos, A.A. Firsov, Nature 438 (2005) 197.
[7] Y. Zhang, Y.-W. Tan, H.L. Stormer, P. Kim, Nature 438 (2005) 201.
[8] K.S. Novoselov, E. McCann, S.V. Morozov, V.I. Falko, M.I. Katsnelson, U. Zeitler, D. Jiang, F. Schedin, A.K. Geim, Nat. Phys. 2 (2006) 177.
[9] S. Das Sarma, S. Adam, E.H. Hwang, E. Rossi, Rev. Mod. Phys. 83 (2011) 407.
[10] M.F. Craciun, S. Russo, M. Yamamoto, J.B. Oostinga, A.F. Morpurgo, S. Tarucha, Nat. Nanotech. 4 (2009) 383.
[11] W. Zhu, V. Perebeinos, M. Freitag, P. Avouris, Phys. Rev. B 80 (2009) 235402.
[12] Y. Liu, S.g Goolaup, C. Murapaka, W.S. Lew, S.K. Wong, ACS Nano 4 (2010) 7087.
[13] W. Bao, Z. Zhao, H. Zhang, G. Liu, P. Kratz, L. Jing, J. Velasco Jr., D. Smirnov, C.N. Lau, Phys. Rev. Lett. 105 (2010) 246601.
[14] A. Kumar, W. Escoffier, J.M. Poumirol, C. Faugeras, D.P. Arovas, M.M. Fogler, F. Guinea, S. Roche, M. Goiran, B. Raquet, ArXiv e-prints (2011), arXiv:1104.1020 [cond-mat.mes-hall].
[15] T. Taychatanapat, K. Watanabe, T. Taniguchi, P. Jarillo-Herrero, Nature 7 (2011) 621.
[16] Liyuan Zhang, Yan Zhang, J. Camacho, M. Khodas, I.A. Zaliznyak, arXiv:1103.6023v1 [cond-mat.str-el].
[17] W. Bao, L. Jing, Y. Lee, J. Velasco Jr., P. Kratz, D. Tran, B. Standley, M. Aykol, S.B. Cronin, D. Smirnov, M. Koshino, E. McCann, M. Bockrath, C.N. Lau, arXiv:1103.6088v1 [cond-mat.mes-hall].
[18] S.H. Jhang, M.F. Craciun, S. Schmidmeier, S. Tokumitsu, S. Russo, M. Yamamoto, Y. Skourski, J. Wosnitza, S. Tarucha, J. Eroms, C. Strunk, arXiv:1106.4995v1 [cond-mat.mes-hall].
[19] E. Peled, Y. Chen, E. Diez, D.C. Tsui, D. Shahar, D.L. Sivco, A.Y. Cho, Phys. Rev. B 69 (2004) 241305 R.
[20] D.-K. Ki, H.-J. Lee, Phys. Rev. B 79 (2009) 195327.
[21] D.-K. Ki, S. Jo, H.-J. Lee, Appl. Phys. Lett. 94 (2009) 162113.
[22] C.H. Lui, Z. Li, Z. Chen, P.V. Klimov, L.E. Brus, T.F. Heinz, Nano Lett. 11 (2011) 164.
[23] B. Karmakar, M.R. Gokhale, A.P. Shah, B.M. Arora, D.T.N. de Lang, A. de Visser, L.A. Ponomarenko, A.M.M. Pruisken, Physica E 24 (2004) 187.